Journal of Solid State Chemistry **144,** 240–246 (1999)
Article ID jssc.1998.8030, available online at http://www.idealibrary.com on IDEAL®

Ordering of Ce^{III}/Ce^{IV} and Interstitial Oxygens in $CeTaO_{4+x}$ ($x \approx 0.17$) Superstructure

John G. Thompson,[1] A. David Rae, Nina Bliznyuk, and Ray L. Withers

Research School of Chemistry, Australian National University, Canberra, ACT 0200, Australia

Received May 15, 1998; in revised form September 8, 1998; accepted September 16, 1998

A structural model for $CeTaO_{4+x}$ ($x \approx 0.17$) or alternately $Ce_4^{III}Ce_2^{IV}Ta_6O_{25}$ (monoclinic, $P2_1$, $a = 7.616(2)$, $b = 16.459(5)$, $c = 7.704(2)$ Å, $\beta = 102.48(2)^\circ$, $Z = 2$) is derived from X-ray powder diffraction data. The starting model was a $3 \times b$ superstructure of $CeTaO_{4+x}$ ($x = 0.0$) with excess oxygen atoms occupying interstices between the Ce atom layers consistent with the electron diffraction determined space group symmetry $P2_1$. Unexpectedly, the four Ce atoms surrounding the interstitial oxygen are not oxidized. During the refinement the model was forced to be chemically plausible by restraining bond valence sums, bond lengths, and O–O distances. This was necessary due to the very weak scattering contribution to the XRD profile by oxygen atoms. The mechanism for oxidation of the subject phase from $CeTaO_{4+x}$ ($x = 0.0$) is discussed and a reason for the limiting composition for this phase is proposed.

INTRODUCTION

$Ce^{III}TaO_4$ is stable in air above 1265°C (1) and at this temperature has the $BaMnF_4$-type structure (2), which is isostructural with the high-temperature form of $LaTaO_4$ (3). Below 1265°C $Ce^{III}TaO_4$ unmixes in air to $Ce^{IV}O_2$ and $Ce^{III}Ta_3O_9$. However, by rapid quenching from its stability field $Ce^{III}TaO_4$ can be obtained as a single phase. At room temperature $Ce^{III}TaO_4$ has the low-temperature $LaTaO_4$-type (4) structure and its crystal structure (monoclinic, $P2_1/c$, $a = 7.6161(3)$, $b = 5.5254(2)(5)$, $c = 7.7588(3)$ Å, $\beta = 100.87(2)^\circ$) has been refined from neutron powder diffraction data (5). It is also isostructural with $Pr^{III}TaO_4$ (4) and $NaNbO_2F_2$ (6).

If $Ce^{III}TaO_4$ is reheated in air at temperatures below 1000°C it has been shown (1) that the reduced phase absorbs oxygen at varying levels according to temperature and annealing regime. The ready oxidation of this phase to mixed Ce^{III}/Ce^{IV} valence states suggested the possibility of electronic and oxygen ion conductivity for these phases (3) though simple resistivity tests indicate that they are electrical insulators.

Thermogravimetric analysis of the oxidation process,

$$CeTaO_4 + x\tfrac{1}{2}O_2 \rightarrow Ce^{III}_{1-2x}Ce^{IV}_{2x}TaO_{4+x},$$

and XRD characterization of reaction product shows that there are three distinct oxidized phases with stability fields as follows:

$$0.50 \geq x \geq 0.48 \ (< 350\text{–}600^\circ C)$$

$$0.17 \geq x \geq 0.06 \ (600\text{–}950^\circ C)$$

$$0.40 \geq x \geq 0.34 \ (950^\circ C\text{–room temperature}).$$

Of the three oxidized phases only the phase at $0.17 \geq x \geq 0.06$ (600°–950°C) showed a simple structural relationship to the reduced phase $Ce^{III}TaO_4$.

A recent TEM study of these oxidized phases (7) showed that the oxidized phase generated when $Ce^{III}TaO_4$ was annealed in air at 650°C possessed a monoclinic unit cell ($a = 7.616(2)$, $b = 16.459(5)$, $c = 7.704(2)$ Å, $\beta = 102.48(2)^\circ$) with probable space group symmetry $P2_1$, i.e., with a $3 \times \mathbf{b}$ superstructure of $Ce^{III}TaO_4$. Roth *et al.* (8) reported a unit cell for $CeTaO_{4.174}$, annealed at 600°C, with $a = 7.617$, $b = 5.491$, $c = 3.851$ Å, $\beta = 102.51^\circ$, in good agreement with the more recent result except that the c axis is halved and the tripling of the b axis is not observed.

Given the close relationship between the $x = 0.0$ and $x \approx 0.17$ structures and the ready reversibility of the oxidation reaction (1), the formation of the $3 \times \mathbf{b}$ superstructure is necessarily due to the uptake of oxygen associated with the oxidation of Ce^{III} to Ce^{IV}, assuming that the bulk of the structure remains more or less intact.

The purpose of this present work is to locate the extra oxygen atoms in $CeTaO_{4+x}$ ($x \approx 0.17$) from X-ray powder diffraction data using the symmetry information derived from the recent TEM study (7) and distance restraints provided by the requirement that the structure is chemically plausible, so as to understand how $CeTaO_{4.0}$ is readily oxidized to $CeTaO_{4.17}$ with minimal structural distortion.

[1] To whom correspondence should be addressed.

0022-4596/99 $30.00

SYNTHESIS AND DATA COLLECTION

$Ce^{III}TaO_4$ was prepared from the component oxides CeO_2 (99.9% Koch–Light) and Ta_2O_5 (99.99% Aldrich). Anhydrous powders were intimately mixed in a mortar and pestle and then pressed into pellets and annealed for 40 h at 1500°C in a platinum crucible, then rapidly quenched to room temperature in water. The process was repeated, with the second annealing being at 1320°C for 16 h. X-ray powder diffraction (XRD) confirmed that the product after the second annealing, a khaki-colored powder, was a single crystalline phase.

$CeTaO_{4+x}$ ($x \approx 0.17$) was prepared by heating $Ce^{III}TaO_4$ ($x = 0$) powder in air at 650°C in a platinum crucible for 16 h, then rapidly cooling in air. Again XRD confirmed that the product was a single phase. Unit cells for both phases were refined from XRD data collected using a Guinier–Hägg camera ($\lambda = 1.5406$) with Si (NBS #640) as an internal standard.

The XRD profile for structure refinement was recorded between 10° and 70° 2θ with 0.05° steps (1200 data spanning 477 reflections) using a Siemens D-5000 X-ray powder diffractometer with Ni-filtered Cu$K\bar{\alpha}$ ($\lambda = 1.5418$ Å) radiation. The specimen for data collection was prepared by thoroughly grinding the powder, loosely front-packing the specimen holder with excess powder, then exposing a flat surface by scraping the excess powder away with a razor blade. This nonstandard method of specimen preparation for the Bragg–Brentano geometry diffractometer was necessary due to a severe preferred orientation problem exacerbated by the extreme linear absorption coefficient of 1709.3 cm^{-1} calculated for this material (9). Other methods proposed to minimize preferred orientation, such as back and side mounting of specimens and mounting on grease (10), proved to be less effective for the present experiment, where >99% of the diffracted beam emanated from the top ~25 μm of the specimen.

DERIVATION OF STARTING MODEL

It was evident from the close similarity between the XRD patterns for the $x = 0.0$ and ~0.17 structures, in particular the similarity of the relative intensities of corresponding reflections, that the change in structure from $CeTaO_4$ to $CeTaO_{4+x}$ ($x \approx 0.17$) involved only small shifts in the metal atoms. The introduction of the extra oxygen atoms into interstices in the $CeTaO_4$ parent structure, with local relaxation of atoms to accommodate the interstitial oxygens, would cause the unit cell to distort and its effective volume to decrease by ~2% (7, 8). The ordering of the interstitial oxygen atoms and the associated relaxation of the surrounding atoms to satisfy bonding requirements and minimize nonbonding interactions caused the formation of the $3 \times \mathbf{b}$ superstructure and the change in space group symmetry to $P2_1$.

For simplicity the composition of the subject phase was assumed to be $Ce^{III}_{1-2x}Ce^{IV}_{2x}TaO_{4+x}$ ($x = \frac{1}{6}$ or 0.1667), which is sufficiently close for the present purposes to the interpolated experimentally determined value for material annealed at 650°C (see Table 1 in Ref. 8). For the unit cell tripled along **b** this corresponds to a formula unit $Ce^{III}_4Ce^{IV}_2Ta_6O_{25}$ with $Z = 2$.

Fractional coordinates for an initial model were obtained from the fractional coordinates of the known parent structure $Ce^{III}TaO_4$ (5) using the transformation

$$x = x_p,\ y = y_p/3,\ z = z_p + \tfrac{1}{4},$$

where p = parent. Note that the 2_1 screw axis now passes through the origin. Six nonequivalent positions in the asymmetric unit of the final structure are obtained from six equivalent positions of the parent structure, e.g.,

$$x_p, y_p, z_p;\quad x_p, y_p + 1, z_p;\quad x_p, y_p + 2, z_p;$$

$$x_p, -y_p + \tfrac{1}{2}, z_p + \tfrac{1}{2};\quad x_p, -y_p + \tfrac{3}{2}, z_p + \tfrac{1}{2};$$

$$x_p, -y_p + \tfrac{5}{2}, z_p + \tfrac{1}{2}.$$

The fractional coordinates of all atoms in the asymmetric unit are given as Model 1 in Table 1.

The incorporation of two additional oxygens per unit cell requires only one site in the asymmetric unit. The equivalents of this site in the parent structure correspond to 12 sites in the unit cell of $CeTaO_{4+1/6}$, i.e., six pairs of equivalent sites. The choices are all equivalent, a particular choice simply selecting the origin and the handedness of the resulting $P2_1$ structure.

The most chemically plausible location for the interstitial oxygens is between the layers of Ce atoms, in particular a vacant tetrahedral site with four of the six Ce atoms in the asymmetric unit at the vertices of the tetrahedron, e.g., Ce1, Ce3, Ce4, and Ce6 (see Table 1). The center of mass of these four Ce atoms is at 0.5, 0.2462, 0.625 and is shown as **X** in the semipolyhedral representations of transformed $CeTaO_4$ shown in Figs. 1a and 1c. However, the equidistant point between these four Ce atoms (shown as + in Figs. 1a and 1c) is located at 0.6073, 0.2421, 0.6566 with Ce–O distances of 2.76 ± 0.01 Å. An oxygen atom at this location has a bond valence sum (11, 12) well below 2 and there is a short O–O contact of 1.78 Å to atom O3 bridging between Ta2 and Ta3.

There are seven oxygen atoms in proximity to this interstitial oxygen site and it was decided that an improved, unbiased initial model would minimize nonbonding interactions. Moving the interstitial oxygen to 0.5640, 0.2389,

TABLE 1
Fractional Coordinates and Bond Valence Sums for Various Structural Models

	Model 1[a]				Model 2[b]				Model 3[c]			
Atom	x	y	z	Bond valence sum	x	y	z	Bond valence sum	x	y	z	Bond valence sum
Ce1	0.3441	0.2576	0.8499	3.70	0.372	0.253	0.824	3.05	0.371(1)	0.254(1)	0.823(1)	3.00
Ce2	0.6559	0.0909	0.1501	2.40	0.652	0.089	0.144	3.85	0.649(1)	0.089(1)	0.142(1)	3.83
Ce3	0.6559	0.0757	0.6501	3.56	0.652	0.078	0.653	3.06	0.651(1)	0.077(1)	0.653(1)	3.10
Ce4	0.3441	0.2424	0.3499	3.76	0.370	0.246	0.363	3.03	0.368(1)	0.247(1)	0.360(1)	3.10
Ce5	0.6559	0.4243	0.1501	2.40	0.665	0.436	0.154	3.93	0.669(1)	0.435(1)	0.154(1)	3.97
Ce6	0.6559	0.4091	0.6501	3.51	0.675	0.398	0.676	3.07	0.674(1)	0.397(1)	0.677(1)	3.10
Ta1	0.1668	0.0890	0.0545	5.20	0.160	0.086	0.061	5.04	0.162(1)	0.086(1)	0.061(1)	5.00
Ta2	0.8332	0.2557	0.9455	5.30	0.851	0.260	0.948	5.07	0.850(1)	0.260(1)	0.949(1)	5.05
Ta3	0.8332	0.2443	0.4455	5.29	0.836	0.251	0.445	5.14	0.836(1)	0.252(1)	0.445(1)	5.07
Ta4	0.1668	0.0777	0.5545	5.20	0.126	0.067	0.541	4.98	0.126(1)	0.067(1)	0.541(1)	5.00
Ta5	0.1668	0.4223	0.0545	5.20	0.169	0.421	0.041	5.04	0.169(1)	0.421(1)	0.040(1)	5.03
Ta6	0.1668	0.4110	0.5545	5.20	0.146	0.421	0.542	5.02	0.147(1)	0.421(1)	0.542(1)	4.96
O1	0.1680	0.0535	0.8044	1.94	0.165	0.045	0.806	2.03	0.161(4)	0.043(2)	0.811(1)	2.03
O2	0.8320	0.2201	0.1956	1.94	0.841	0.230	0.203	1.90	0.833(9)	0.239(3)	0.198(2)	1.99
O3	0.8320	0.2799	0.6956	2.05	0.897	0.281	0.714	1.95	0.889(2)	0.288(3)	0.710(2)	2.00
O4	0.1680	0.1132	0.3044	2.05	0.165	0.108	0.305	1.98	0.163(9)	0.107(2)	0.318(4)	1.99
O5	0.1680	0.3868	0.8044	2.05	0.164	0.390	0.801	1.97	0.169(9)	0.391(2)	0.800(3)	2.00
O6	0.1680	0.4465	0.3044	2.05	0.165	0.446	0.304	2.00	0.169(7)	0.449(3)	0.303(1)	1.99
O7	0.0568	0.1956	0.9567	1.94	0.058	0.193	0.972	1.97	0.057(3)	0.192(2)	0.980(10)	2.01
O8	0.9432	0.0290	0.0433	1.87	0.934	0.033	0.045	1.97	0.938(3)	0.030(2)	0.036(9)	2.02
O9	0.9432	0.1377	0.5433	1.91	0.937	0.142	0.542	2.00	0.932(7)	0.142(3)	0.538(7)	1.97
O10	0.0568	0.3044	0.4567	1.94	0.053	0.310	0.458	1.99	0.051(5)	0.311(3)	0.457(9)	2.05
O11	0.9432	0.3623	0.0433	1.87	0.960	0.358	0.064	2.07	0.952(5)	0.360(2)	0.061(6)	2.02
O12	0.9432	0.4710	0.5433	1.90	0.919	0.461	0.602	2.18	0.928(7)	0.464(1)	0.618(2)	2.01
O13	0.3823	0.1614	0.0812	2.16	0.388	0.148	0.086	1.97	0.387(2)	0.148(1)	0.066(8)	2.00
O14	0.6177	0.3281	0.9188	2.17	0.625	0.331	0.957	2.09	0.626(2)	0.325(1)	0.986(3)	1.98
O15	0.6177	0.1719	0.4188	2.23	0.642	0.159	0.383	2.09	0.632(6)	0.164(2)	0.374(4)	2.05
O16	0.3823	0.0053	0.5812	2.23	0.369	0.006	0.615	1.97	0.366(6)	0.009(2)	0.620(5)	2.02
O17	0.3823	0.4947	0.0812	2.00	0.397	0.494	0.060	2.09	0.397(3)	0.495(2)	0.074(6)	2.04
O18	0.3823	0.3386	0.5812	2.33	0.372	0.366	0.544	2.14	0.377(5)	0.375(2)	0.516(6)	2.03
O19	0.3338	0.0028	0.1171	2.09	0.360	−0.001	0.101	1.97	0.379(4)	0.013(2)	0.083(3)	2.01
O20	0.6662	0.1695	0.8829	2.13	0.690	0.159	0.915	2.04	0.674(5)	0.162(2)	0.911(2)	2.02
O21	0.6662	0.3305	0.3829	2.09	0.671	0.338	0.347	2.00	0.678(4)	0.347(3)	0.370(7)	2.00
O22	0.3338	0.1639	0.6171	2.26	0.299	0.149	0.626	2.08	0.315(3)	0.145(2)	0.627(6)	1.97
O23	0.3338	0.3361	0.1171	2.21	0.348	0.342	0.124	1.88	0.330(5)	0.334(2)	0.120(5)	2.00
O24	0.3338	0.4972	0.6171	2.10	0.321	0.513	0.621	1.99	0.318(3)	0.514(3)	0.619(5)	2.00
O25[d]	0.5640	0.2389	0.6429	1.22	0.567	0.242	0.637	1.94	0.568(2)	0.257(1)	0.633(1)	2.01

[a] $CeTaO_{4.0}$ parent structure coordinates (Santoro *et al.* 1980) transformed so that $x = x_p$, $y = y_p/3$, $z = z_p + \frac{1}{4}$.
[b] Coordinates from chemically constrained dataless refinement.
[c] Coordinates from chemically constrained XRD profile refinement.
[d] Interstitial oxygen.

0.6429 (shown as the small grey sphere in Fig. 1a and 1c) gives O–O distances of 2.104 Å for O–O3, 2.134 Å for O–O18, 2.118 Å for O–O22, 2.161 Å for O–O15, and 2.169 Å for O–O20 with two longer distances of 2.543 Å for O–O14 and 2.751 Å for O–O21. In this position the bond valence sum for the interstitial oxygen, with no Ce atom displacements from their parent positions, is 1.22 when all the four surrounding Ce atoms are Ce^{III} (Ce–O distances (Å) of 2.569 (Ce1), 2.773 (Ce3), 2.504 (Ce4), and 2.886 (Ce6), respectively). The bond valence sum is even less if some of these Ce are Ce^{IV}. Obviously the O–O contacts have to increase by at least 0.4 Å while at least some of the interstitial O–Ce bond lengths have to decrease.

The remaining feature of the starting model to be determined is which two out of the six independent Ce sites are the Ce^{IV} sites. This was resolved by comparative refinement of the various options and is treated below.

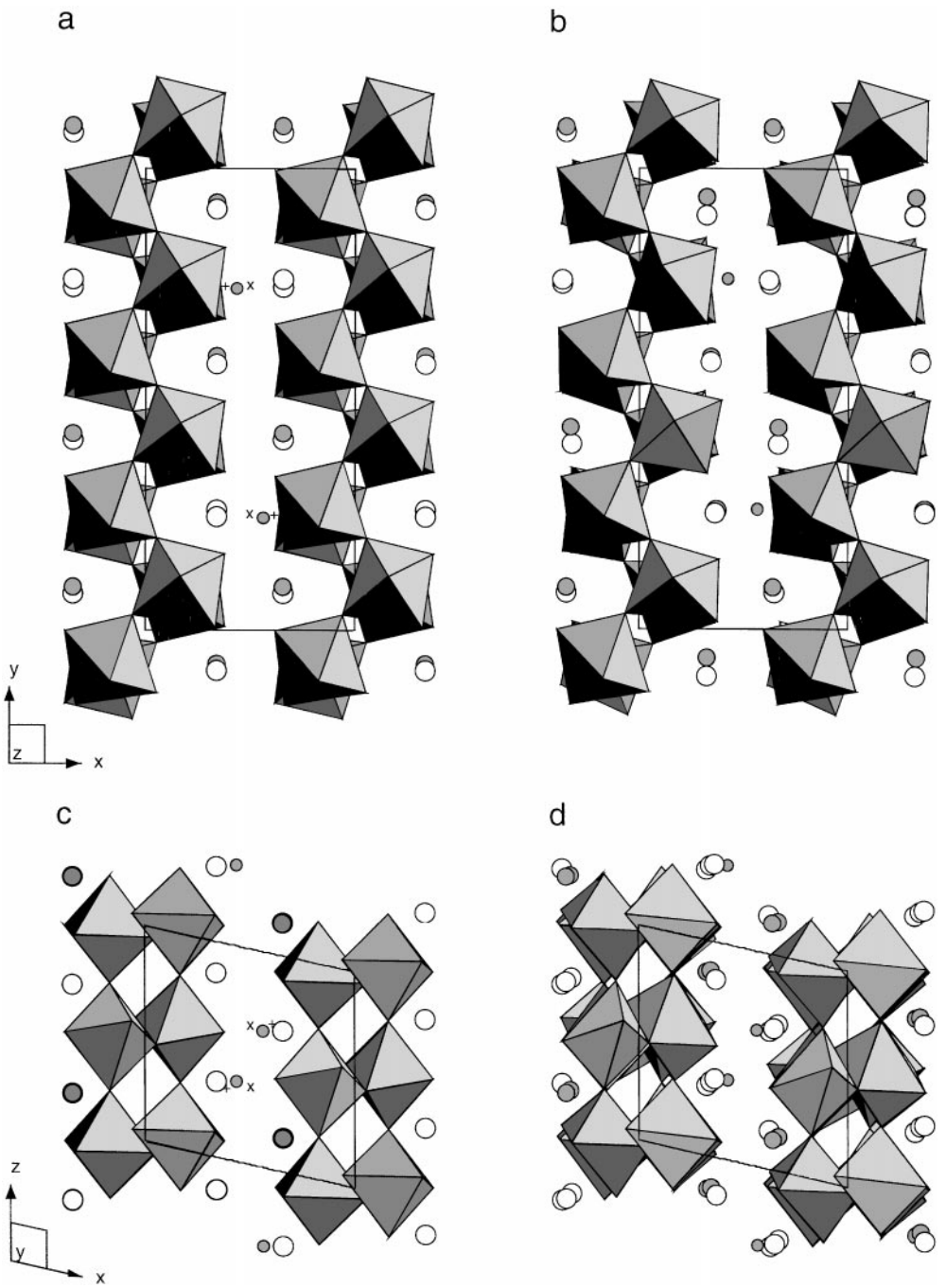

FIG. 1. Schematic semipolyhedral representations of the $CeTaO_{4.17}$ parent starting model, Model 1, along [001] (a) and [010] (c), juxtaposed to the final refined model, Model 3, along the same directions (b, d). The fractional coordinates x_p, y_p, z_p (p = parent) of the $Ce^{III}TaO_4$ (2) parent structure have been tranformed so that $x = x_p$, $y = y_p/3$, $z = z_p + 1/4$ and set in the observed unit cell for $CeTaO_{4.17}$. **X** marks the location of the center of mass of the four Ce^{III} atoms, Ce1, Ce3, Ce4, and Ce6, while + marks the equidistant point. The two Ce^{IV} atoms, Ce2 and Ce5, are shown as grey spheres, the four Ce^{III} atoms as larger white spheres, and the interstitial oxygen, O25, as a smaller lighter sphere.

STRUCTURE REFINEMENT

The only experimental data for $CeTaO_{4.17}$ available to us are from X-ray powder diffraction. These data are dominated by the metal atoms Ce and Ta ($Z = 58$ and 73, respectively), which makes impossible the direct observation of the interstitial oxygen atom and unconstrained refinement of oxygen ($Z = 8$) atom positions. Furthermore, even if the

scattering by all the atoms was on a scale similar to that for neutron diffraction, since the structure is pseudo-centrosymmetric and there are 37 independent atoms in the asymmetric unit, unconstrained refinement using the Rietveld method is unlikely to be successful. Therefore, it was necessary to use distance restraints based on the assumption that the structure of $CeTaO_{4.17}$ should be chemically plausible.

Derivation of a chemically plausible starting model, including selection of the best model of Ce^{IV} ordering, discussed above, was performed by least-squares refinement methods using RAELS96 (13), without intensity data, using the following refinement restraints.

1. Atoms to stay near the positions determined by the previous cycle.
2. Bond valence sums approach their ideal values.
3. O–O contacts less than 2.55 Å to approach this value.
4. The six Ta–O bonds per TaO_6 outside the range 1.91–2.08 Å to approach the nearest limit.
5. Ce^{IV}–O contacts less than 2.20 Å to approach this value.
6. Ce^{III}–O contacts less than 2.32 Å to approach this value.
7. Certain of the interstitial O–Ce contacts to approach equality until the final cycle. This last constraint speeds convergence by restricting the initial shift of the interstitial O atom.

The two criteria to be satisfied were (a) complying as far as possible with the above restraints while (b) minimizing the deviation from the initial $CeTaO_4$-derived model. The problem was defined in terms of residuals, Δ_i, corresponding to geometry constraints where $\sum_i w_i \Delta_i^2$ was minimised.

When the Ce^{IV} atoms were located on two of the four Ce sites surrounding the interstitial oxygen, the associated Ce^{IV}–O distances were restrained to be equal until the final cycle. Four such models were tried (Ce1, Ce4), (Ce3, Ce4), (Ce3, Ce4), (Ce3, Ce6), before it was realized that the most plausible model located the Ce^{IV} atoms on the Ce2 and Ce5 sites, i.e., where the four Ce^{III} sites are in contact with the interstitial oxygen while the two Ce^{IV} sites are not.

It followed that the $\sim$2% cell volume reduction upon addition of interstitial oxygen is associated with the shrinking of Ce–O contacts around the Ce^{IV} sites to satisfy the bonding requirements. Increasing the oxygen coordination about a Ce^{IV} site would inhibit any shrinkage. The model, as we see it, can be simply described as a displacement of oxygen atoms away from the intersitial oxygen atom toward Ce^{IV} atoms. To satisfy the bonding requirements of the interstitial oxygen atom the four Ce^{III} atoms, to which it is bonded, have to move less than for the other models.

This model was initially restrained so that the interstial oxygen distances to Ce1 and Ce4 approach equality. These ended up as the two shortest Ce^{III}–O bonds, 2.310 and 2.314 Å, while Ce3–O and Ce6–O were 2.799 and 2.631 Å, respectively. The fractional coordinates and bond valence sums (11, 12) for the preferred model, which to this point were derived without reference to the XRD data, are also given as Model 2 in Table 1. The largest displacements from the starting $CeTaO_4$-derived model, Model 1, were for atoms O12, O15, O17, O20, and O22 which were 0.55, 0.74, 0.55, 0.57, and 0.52 Å, respectively, the remainder being less than 0.5 Å.

Having optimized bond valence sums and nonbonding interactions the model was tested against the experimental data. Using the program GSAS (14) the XRD profile was refined using only 15 non-atomic variables (scale, zero correction, unit cell (4), profile (pseudo Voigt type 2-GW, LY and asym), background (cosine fourier series #2–3 coefficients), isotropic thermal parameters with like atoms constrained to be equal). The refinement converged to give R_p 0.059, wR_p 0.079 and reduced χ^2 0.441.

While the difference profile indicated a remarkably good fit of the model to the data, there were still some unsatisfactory mismatches in intensities. Being aware of the extreme susceptibility of the specimen to preferred orientation, we attempted to model any remaining preferred orientation using the available function. Up to 0.001 reduction in the R-factors was achieved by the addition of this further variable but this did not appear to be the principal cause of the mismatch.

In order to run a chemically restrained least-squares refinement of the model against the XRD data, we used the derived observed intensities from the Rietveld refinement (without modeling preferred orientation) as input for RAELS96. The refinement, using the same chemical and distance restraints listed above, converged at $R(F) = 0.047$, $R(F^2) = 0.063$, and w$R(I) = 0.040$. Anisotropic thermal displacement parameters were applied with like atoms constrained to maintain the parent $P2_1/c$ structure symmetry relationships. A preferred orientation correction, corresponding to $\{101\}$ and $\{010\}$ forms of faces, was applied with improved statistics, $R(F) = 0.041$, $R(F^2) = 0.048$, and w$R(I) = 0.033$. The fractional coordinates and bond valence sums for the final refined model are listed in Table 1 as Model 3 and shown juxtaposed to the parent structure in Fig. 1. Model 3 is little changed from the dataless refinement, Model 2, with O14, O18, O21, and O25 shifted 0.24, 0.27, 0.23, and 0.25 Å, respectively, the remainder shifting less than 0.2 Å. Anisotropic thermal displacement parameters for Model 3 are listed in Table 2.

The above model was input into GSAS and nonatomic variables were refined, including preferred orientation. The refinement converged to give R_p 0.057, wR_p 0.074, and reduced χ^2 0.382. The observed, calculated, and difference profiles are shown in Fig. 2.

TABLE 2
Anisotropic Thermal Displacement Parameters for Model 3

Atom	U^{11}	U^{22}	U^{33}	U^{12}	U^{13}	U^{23}	U_{equiv}[a]
Ce1	0.045(2)	0.040(2)	0.058(2)	−0.003(2)	0.014(2)	0.000(1)	0.047(1)
Ce2	0.045(2)	0.040(2)	0.058(2)	0.003(2)	0.014(2)	0.000(1)	0.047(1)
Ce3	0.045(2)	0.040(2)	0.058(2)	−0.003(2)	0.014(2)	0.000(1)	0.047(1)
Ce4	0.045(2)	0.040(2)	0.058(2)	0.003(2)	0.014(2)	0.000(1)	0.047(1)
Ce5	0.045(2)	0.040(2)	0.058(2)	0.003(2)	0.014(2)	0.000(1)	0.047(1)
Ce6	0.045(2)	0.040(2)	0.058(2)	−0.003(2)	0.014(2)	0.000(1)	0.047(1)
Ta1	0.011(1)	0.007(1)	0.013(1)	0.000(1)	0.006(1)	0.002(1)	0.010(0)
Ta2	0.011(1)	0.007(1)	0.013(1)	0.000(1)	0.006(1)	−0.002(1)	0.010(0)
Ta3	0.011(1)	0.007(1)	0.013(1)	0.000(1)	0.006(1)	0.002(1)	0.010(0)
Ta4	0.011(1)	0.007(1)	0.013(1)	0.000(1)	0.006(1)	−0.002(1)	0.010(0)
Ta5	0.011(1)	0.007(1)	0.013(1)	0.000(1)	0.006(1)	0.002(1)	0.010(0)
Ta6	0.011(1)	0.007(1)	0.013(1)	0.000(1)	0.006(1)	−0.002(1)	0.010(0)
O1–O25	0.079(4)						

[a] $U_{equiv} = \frac{1}{3} S_{ij} U^{ij} a_i^* a_j^* a_i \cdot a_j$.

DISCUSSION

The refined model for $CeTaO_{4.17}$ is, by virtue of the chemical constraints, necessarily chemically plausible and conforms to the space group symmetry observed by TEM (7). The choice of the Ce2 and Ce5 sites for the two Ce^{IV} atoms, neither of which are coordinated to the interstitial oxygen O25, is based on the rationale that this model requires the least displacement of atoms from the reduced $Ce^{III}TaO_4$ structure from which it is formed.

The introduction of the interstitial oxygen displaces neighbouring oxygens simultaneously away from the interstitial site and the Ce^{III} atoms to which they are bonded towards the Ce^{IV} atoms to which they are also bonded. This displacement of the neighbouring oxygens serves to satisfy the changed bonding requirements of both the Ce^{III} atoms, which now have higher coordination by oxygen, and the Ce^{IV} atoms, which have the same coordination but require an average shortening of Ce–O bonds by $\sim$0.2 Å to satisfy their bond valence (11, 12).

Figure 3 shows the change in coordination environments upon oxidation of Ce1 and Ce2, representative of Ce^{III} and Ce^{IV} sites, respectively, in the final model. The introduction of the interstitial oxygen into the coordination sphere of Ce1 results in an increase in most of the Ce–O bond lengths while the oxidation of Ce2 from Ce^{III} to Ce^{IV} leads to noticeable bond shortening, the latter effect dominating the changes in unit cell dimensions. There is a $\sim$0.7% reduction in the b_p and c_p cell dimensions and a 1.5° increase in β, corresponding to a volume decrease of 2.1%, while the density increases by 2.8% from 3.985 to 4.098 g.cm^{-3} with the addition of the interstitial oxygens. Throughout the oxidation process the octahedral tantalate framework remains relatively unchanged (see Fig. 1).

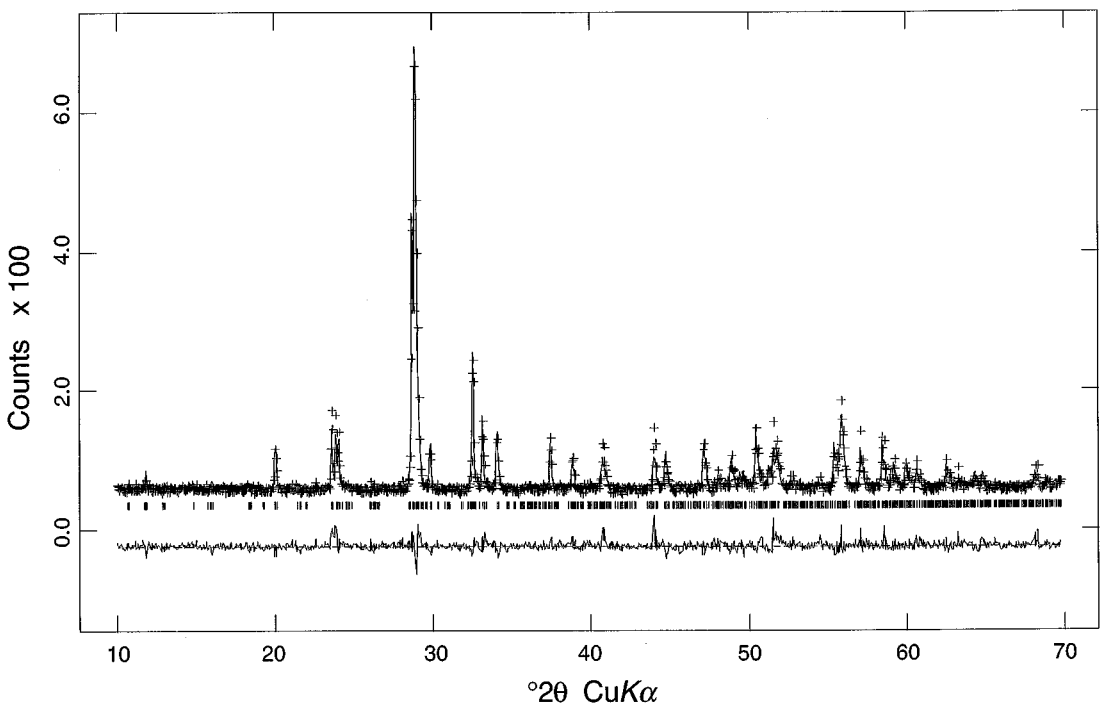

FIG. 2. Observed, calculated, and difference profiles from the Rietveld refinement of the XRD data for $CeTaO_{4.17}$ between 10° and 70° 2θ. The observed data points are shown as + and the calculated profile as a continuous line.

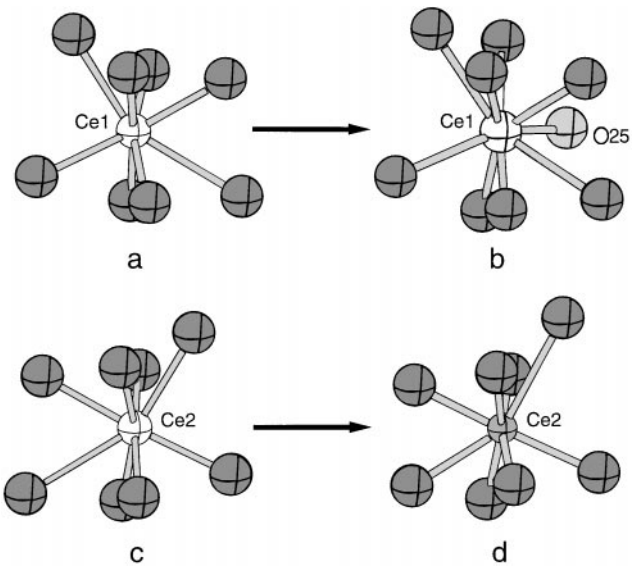

FIG. 3. Ball and stick representations of the coordination environments, before and after oxidation, of Ce1, (a, b), and Ce2, (c, d). Ce^{III} and Ce^{IV} are represented as white and grey spheres, respectively. The interstitial oxygen, O25, is labeled.

The mechanism of oxidation of $Ce^{III}TaO_4$ to $CeTaO_{4.17}$ presumably involves the diffusion of oxygen atoms between the Ce atom layers parallel to the **bc** plane. Figure 4 shows a schematic representation of $Ce^{III}TaO_4$ with a path of minimum structural disruption traversing all the interstitial sites. In the $CeTaO_{4.17}$ superstructure only $\frac{1}{6}$ of these sites are filled, corresponding to oxidation of $\frac{1}{3}$ of the Ce^{III} atoms. The upper limit of oxygen content for this solid solution phase, reported as $x = 0.17$ or $\frac{1}{6}$, may be explained as the maximum oxygen uptake in the interstitial sites which allows the intersitial oxygens to be coordinated by Ce^{III} atoms only.

Given the minimal bond breaking and reforming involved in the formation of the $CeTaO_{4.17}$ superstructure and the relatively small displacements of atoms from the reduced phase structure, it is easy to understand why this phase is so readily formed at temperatures as low as 600°C and why the phase transition is reversible.

What is not so easily understood is why the stable phase at temperatures between 350° and 600°C ($0.50 \geq x \geq 0.48$) (1) is effectively fully oxidized and, unlike $CeTaO_{4.17}$, shows no simple relationship to the reduced phase (7). One would expect that the same oxygen diffusion mechanism would apply to the formation of this phase from $Ce^{III}TaO_4$. However, until the unit cell relationship between the low-temperature, fully oxidized phase $Ce^{IV}TaO_{4.5}$ and $Ce^{III}TaO_4$ is identified its structure is likely to remain a mystery.

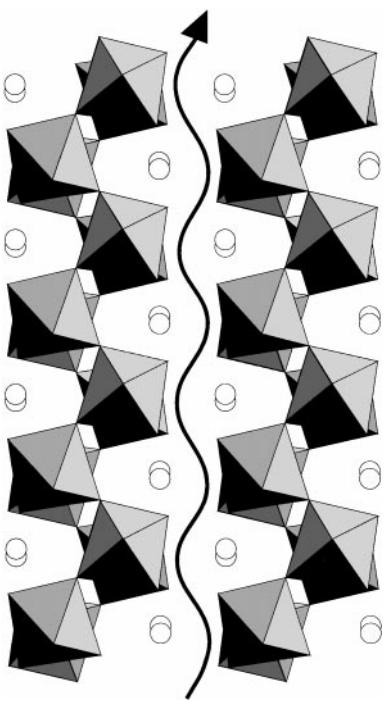

FIG. 4. A schematic semipolyhedral representation of $Ce^{III}TaO_4$ with a path of minimum structural disruption for oxygen atom diffusion which traverses all the interstitial sites.

REFERENCES

1. T. Negas, R. S. Roth, C. L. McDaniel, H. S. Parker, and C. D. Olson, *Mater. Res. Bull.* **12,** 1161 (1977).
2. E. T. Keve, S. C. Abrahams, and J. L. Bernstein, *J. Chem. Phys.* **51,** 4928 (1969).
3. R. J. Cava and R. S. Roth, *J. Solid State Chem.* **36,** 139 (1981).
4. T. A. Kurova and V. B. Akesandrov, *Dokl. Akad. Nauk. SSSR* **201,** 1095 (1971).
5. A. Santoro, M. Marezio, R.S. Roth, and D. Minor, *J. Solid State Chem.* **35,** 167 (1980).
6. S. Andersson and J. Galy, *Acta Crystallogr. Sect. B* **25,** 847 (1969).
7. G. Drew, R. L. Withers, A.-K. Larsson, and S. Schmid, *J. Solid State Chem.* **140,** 20 (1998).
8. R.S. Roth, T. Negas, H. S. Parker, D. B. Minor, and C. Jones, *Mater. Res. Bull.* **12**, 1173 (1977).
9. A.J.C. Wilson, Ed., "International Tables for Crystallography," Vol. C. Kluwer Academic, Dordrecht, 1992.
10. D. L. Bish and R. C. Reynolds, Jr., *Modern Powder Diffraction*, Ch. 4 *in* "Reviews in Mineralogy" (D. L. Bish and J. E. Post, Eds.,), Vol. 20, Chap. 4. Mineralogical Soc. of Amer., Washington, DC, 1989.
11. I. D. Brown and D. Altermatt, *Acta Crystallogr. Sect. B* **41,** 244 (1985).
12. N. E. Brese and M. O'Keeffe, *Acta Crystallogr. Sect. B* **47,** 192 (1991).
13. A. D. Rae, "RAELS96. A Comprehensive Constrained Least-Squares Refinement Program." Research School of Chemistry, Australian National University, 1996.
14. A. C. Larson and R. B. von Dreele, "GSAS. The General Structure Analysis System." Los Alamos, 1991.